Sizes and Second Virial Coefficients of Miktoarm Star Polymers

ARTICLE *in* MACROMOLECULES · JANUARY 2000

Impact Factor: 5.8

1 AUTHOR:

Costas Vlahos

University of Ioannina

34 PUBLICATIONS **374** CITATIONS

SEE PROFILE

Sizes and Second Virial Coefficients of Miktoarm Star Polymers

Ana M. Rubio, Pilar Brea, and Juan J. Freire*

Departamento de Química Física, Facultad de Ciencias Químicas, Universidad Complutense, 28040 Madrid, Spain

Costas Vlahos

Department of Chemistry, University of Athens, Panepistimiopolis, Zografu, 15771 Athens, Greece

Received August 5, 1999; Revised Manuscript Received October 25, 1999

ABSTRACT: An off-lattice bead model with a hard-sphere potential between interacting units has been used to characterize the sizes and second virial coefficients of miktoarm star polymers A_xB_y using Monte Carlo simulations. These stars are composed of $f = x + y$ branches. Each arm contains N_A units of type A or N_B of type B. The number of units in each arm is determined by the total number of units N, and the compositional fraction, $\Phi_B = yN_B/N$. We assume that each one of two types of units can be immersed in a good solvent (which we associate with repulsive interactions between the corresponding chain units AA or BB) or in a Θ solvent (in which case,we do not consider interaction between these units). Repulsive interactions are always used between polymer units of different types (AB). The numerical sizes and second virial coefficients are analyzed in terms of some ratios. These ratios are obtained with the values of the miktoarms and those of linear diblock copolymers with the same compositional fraction. We also analyze the interpenetration factors that combine these two different properties for a given type of star molecule. The ratios of second virial coefficients are compared with recent theoretical estimations.

Introduction

Uniform star polymer chains composed of branches of identical length (or molecular weight) and chemical composition have received a great amount of attention due to their special properties, which can reveal the essential effects of branching and lead to a better understanding of other systems, such as network or even colloidal particles.[1,2] Some varieties of star copolymer chains are also interesting and have been recently synthesized. Miktoarm stars[3] A_xB_y are comprised of a total of N monomeric (or, in the case of theoretical models, coarse-grained) units distributed into $f = x + y$ branches (functionality f), where the x branches are each composed of N_A units of type A and the y branches are each composed of N_B units of type B. The ratio between the molecular weights of the A and B branches defines the compositional fraction $\Phi_B = yN_B/(xN_A + yN_B)$. In our previous work, we have investigated the single-chain conformational properties of this type of star polymer using renormalization group theory[4] and a simple perturbation scheme in which size-related properties may be calculated. The values of the interaction parameters at the fixed points u_{AA}*, u_{BB}*, and u_{AB}* define the solvent regimes for the A and B units as well as the nature of the heterointeractions, and these parameters are obtained up to first order in the expansion parameter $\epsilon = 4 - d$ (d is the space dimension). The results obtained were found to be in qualitative agreement with Monte Carlo simulations[5] for analogous cases.

The description of binary polymer−polymer interactions is, on the other hand, useful to establish a bridge between single- and many-chain conformational properties. Douglas and Freed performed renormalization group calculations using an exponentiation method[6] to study interactions of linear and uniform star chains in a good solvent. The results can be compared with experimental results for the osmotic second virial coefficient of polymer solutions, A_2, and with simulation values. These simulation values can be obtained by computing the intermolecular interaction between a pair of flexible molecules[7] whose centers of mass are kept at distance r, in different randomly chosen conformations and with a given choice of Euler angles that define their mutual orientation and, then, evaluating

$$\Gamma_2 = A_2M^2/N_{AV} = 2\pi\int_0^\infty [1 - \langle e^{-U(r)/kT}\rangle]r^2\, dr \quad (1)$$

where M is the molecule's molecular weight, N_{AV} is Avogadro's number, kT is the Boltzmann factor, and $U(r)$ is the intermolecular interaction. In the present case, each molecule consists of a star chain with N units that, in the good solvent regime, interact through a repulsive potential. A Monte Carlo average is performed over different orientations and conformations.

In practice, a comparison between the different results may be expressed in terms of a nondimensional interpenetration factor

$$\Psi^* = 2\Gamma_2/(4\pi\langle S^2\rangle)^{3/2} \quad (2)$$

where $\langle S^2\rangle$ is the mean-square radius of gyration of the chain. For a given solvent regime, Ψ* should reach the asymptotic long-chain value (the experimental data are usually obtained from high-molecular-weight samples; the renormalization group theory assumes infinitely long chains, and the Monte Carlo results are conveniently extrapolated to infinite N). The theory is in good agreement with experiment and Monte Carlo calculations for linear chains[8] in a good solvent although the Ψ* become unphysically negative for stars with $f \geq 18$. In fact, the renormalization group theory can only reproduce the experimental data for star chains of low functionality, $f \leq 6$. Some Monte Carlo results for uniform star chains[9−11] in a good solvent have also recently been obtained. The Monte Carlo data for stars

10.1021/ma9913156 CCC: $19.00
Published on Web 12/11/1999

Scheme 1. Architecture and Compositional Variables of a Miktoarm Star and Considered Solvent Regimes[a]

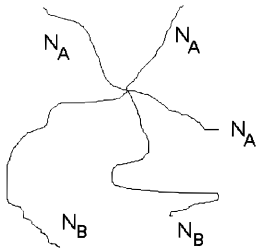

x branches of N_A units A
y branches of N_B units B
$\Phi_B = yN_B/(xN_A+yN_B)$

[a] Possible solvent cases: case a, A and B units in a common good solvent; case b, A and B units in a common Θ (ideal) solvent; and case c, Θ solvent for the A units and a good solvent for the B units.

having up to 18 arms are in good agreement with the experimental data.

The renormalization group scheme employed to study the single-chain properties of miktoarms considering different solvent regimes for the A and B units has also been recently applied to obtain second virial coefficients of the these polymers.[12] The miktoarm molecules are defined in terms of f, x, and Φ_B. The theoretical data are compared with experimental data in terms of the ratios

$$g_A = (A_2)_{\text{mikto}}/(A_2)_{\text{diblock}} \tag{3a}$$

where the "mikto" and "diblock" subindices refer to the A_2 values corresponding to the interaction of two miktoarm or two linear diblock copolymers, respectively, with both the linear chains and the miktoarm stars having the same total number of units, N, and compositional fractions, Φ_B (homologous molecules). Of course, one can also consider similar ratios for the averaged squared radii of gyration

$$g_S = \langle S^2 \rangle_{\text{mikto}}/\langle S^2 \rangle_{\text{diblock}} \tag{3b}$$

Several sets of fixed-point interaction parameters u_{AA}*, u_{BB}*, and u_{AB}* have been employed to describe the different interesting solvent regimes for the A and B units. These sets are the same as that in the previous single-chain study of miktoarms.[4] Of course, some of the cases actually correspond to uniform homopolymer star chains in a good solvent. In these cases, it is observed that the theoretical ratios g_A are clearly smaller that the experimental data. For moderate functionalities, the results are even smaller than those obtained with the Douglas and Freed method, although they are always positive, even for large f. The differences are somehow alleviated by considering for these cases a closed form for A_2 in terms of the interaction parameters, according to the procedure previously established by Kosmas and Kosmas,[13] although important differences between theory and simulation data still persist.

In this paper, we perform a detailed simulation study of second virial coefficients for miktoarm molecules, considering a great variety of different choices; see Scheme 1. Our purpose is to give the first accurate estimations of these magnitudes that can also serve as references to elaborate more accurate theoretical predictions for these and other possible cases. We consider three cases corresponding to common good, common Θ, and selective solvents, defined according to a hard-sphere potential acting between the individual units. In the common good solvent, the long-range homo- and heterointeractions between all the units are similar. In the common Θ solvent case, we consider the hypothetical situation for which both the binary inter- and intramolecular homointeractions for the A or the B units are effectively canceled so that the only effective binary long-distance interactions between units are the heterointeractions AB. Although it is in principle possible to achieve experimental conditions corresponding to a common Θ solvent for two different polymers (probably employing an appropriate mixture of solvents with the right composition at a given temperature), the main interest of the common Θ solvent case in the present case is that allows us a direct comparison with theory. It should be, nevertheless, remarked, that this ideal description of the Θ behavior cannot describe the purely steric core interactions for star chains, which give raise to the well-known stretch effects.[1,2] According to these effects, the radius of gyration of a homopolymer star in a real Θ solvent is always greater than the theoretical result for the ideal star without long-distance intramolecular interactions. For the case of a selective solvent, we consider that the A binary homointeractions between A units have been effectively canceled (Θ solvent for A) while the homointeractions for the B units are similar to the heterointeractions (good solvent for B).

Numerical and Simulation Methods

We generate conformations of a miktoarm with the given values of f, x, and Φ_B and composed of N beads joined by randomly oriented bonds, whose lengths are not constant but are chosen from a Gaussian distribution with a root-mean-square value b (our length unit). In the absence of any intramolecular potential, these chains exactly correspond to the unperturbed Gaussian chain model. However, we include a long-range intramolecular and intermolecular hard-sphere potential so that conformations where two nonneighboring units are placed at distances smaller than the sphere diameter value σ are discarded if these units suffer a net repulsion. Namely, we consider repulsions between all units for a good solvent, $\sigma_{AA} = \sigma_{BB} = \sigma_{AB} = \sigma$ (case a), we consider only repulsions to describe the heterointeractions AB for a common Θ solvent (where binary homointeractions are effectively canceled) $\sigma_{AA} = \sigma_{BB} = 0$, and $\sigma_{AB} = \sigma$ (case b), and finally, we consider repulsions to mimic the heterointeractions and to describe the interactions between B units for selective solvents, $\sigma_{AA} = 0$ and $\sigma_{BB} = \sigma_{AB} = \sigma$ (case c). These sets have been chosen to be consistent with our description of the homo- and heterointeractions that correspond to each one of the considered cases.

We have previously optimized the value of σ for linear homopolymers in the good solvent regime.[11] This value has been set so that (1) it gives numerical values for the exponent ν of the scaling laws

$$\langle S^2 \rangle = A_S(f, x, \Phi_B)N^{2\nu} \tag{4a}$$

$$\Gamma_2 = A_\Gamma(f, x, \Phi_B)N^{3\nu} \tag{4b}$$

that are close to the theoretical result $\nu = 0.588$ and that are mutually consistent between them and (2) it gives values of Ψ* showing the weakest variation with N. These conditions are met for $\sigma = 0.55$. This result is also consistent with calculations based in theoretical arguments[14] and has been employed in some previous simulations with the same model.[15] Here, we adopt the same value to describe repulsive interac-

tions for miktoarms with any value of f, x, and Φ_B. We build a first valid conformation of the sample complying with this nonoverlapping requirement. Other conformations are generated by selecting a bond vector in the previous conformation and resampling its components from the Gaussian distribution, with zero mean and square deviation equal to $(^1/_3)b^2$. In cases *a* and *c*, the rest of the chain up to its closest end is rotated by means of three randomly chosen Euler angles and then translated to connect with this new bond (Pivot algorithm[16]). (We should mention that in some of the simulations, namely, those corresponding to the common Θ solvent, case b, that correspond to denser chains, we have avoided the rotation and the short part of the chain has been simply translated to connect to the new bond. Both algorithms, however, are expected to be similarly efficient for all of the present cases). Subsequently, the new conformation is accepted or not depending on the hard-sphere criterion. In this screening of the overlapping condition, we consider again the previous conformation if a new conformation cannot be accepted. Intramolecular averages as $\langle S^2 \rangle$ are simply evaluated as arithmetic means over the results obtained for the radius of gyration from the positions of units in the accepted conformations. In the second virial coefficient calculations, we consider pairs of accepted conformations corresponding to two samples that are simultaneously generated.[10,17] We adopt several values of the distance between the centers of masses. Maintaining the original coordinates of the first chain, we place the center of masses of chain 2 on a random point of the surface of the sphere of radius r, which is centered in the center of masses of chain 1. We check whether the resulting configuration, constituted by a pair of conformations, is accepted or not, according to the intermolecular hard-sphere potential acting on the appropriate pairs of units of chains 1 and 2. We evaluate the fraction of pairs of conformations accepted in the sample for each given value of distance r, $\langle f_a(r) \rangle$. Finally, we obtain Γ_2 by numerical integration

$$\Gamma_2 = 2\pi \int_0^\infty [1 - \langle f_a(r) \rangle] r^2 \, dr \qquad (5)$$

Eight independent samples (four independent sample pairs for the evaluation of Γ_2) are actually considered, and the final quantities are obtained as further averages over the samples means. Each sample is composed of 400 000 Pivot moves for cases *a* and *b* and 200 000 for case c (selective solvent). We have verified that we do not need to introduce moves to allow for an initial equilibration. All of these specifications have allowed us to obtain final results for the chain sizes and second virial coefficients with uncertainties that generally do not exceed 0.5%. Acceptance fractions are about 50% for case a, 85% for case b, and 75% for case c, for a diblock copolymer. These fractions suffer a decrease of about a 5% in each solvent case for stars with $f = 6$. This decrease of about 10% for stars with $f = 12$.

Results and Discussion

Table 1 contains the results of our numerical data for $\langle S^2 \rangle$ and Γ_2 corresponding to chains of different topologies and different values of N, but with $\Phi_B = 0.5$ for the three cases of common good, common Θ, and selective solvents. Similar results have been obtained for different values of the compositional fractions $\Phi_B =$ 0.1, 0.2, 0.3, 0.4, 0.6, 0.7, 0.8, and 0.9, also with the same variety of architectures, the same range of values of N, and considering the three solvent cases. Limit values for $\Phi_B = 0$ and 1 are obtained from equivalent cases when possible or derived from other results as it will be described below.

Comparing the results for the radii of gyration corresponding to the same value of the total number of units, we verify the obvious decrease of size when the number of arms increases. For a given topology and same N, it is also verified that the highest size corresponds to case a (good solvent). The smallest size corresponds to case b, ideal solvent, whereas the case c (selective solvent) exhibits intermediate sizes in good agreement with the qualitative expectations. Similar features are shown by the second virial coefficients as they are directly related with the sizes and the number of intermolecular interactions that are only present for the heterointeractions and the arms immersed in a good solvent.

It can also be easily understood that, at $\Phi_B = 0.5$, and considering the same total number of units N, the same total number of arms f, and the same solvent case, the miktoarm stars with $x = y$ show the smallest radius of gyration, because $x \neq$ y implies nonuniform stars with different arm lengths and, consequently, arrangements of units more similar to linear chains of higher sizes (see Scheme 1). In the case of selective solvents, the highest sizes at $\Phi_B = 0.5$ correspond to the chains with $x > y$ that possess the longest arms of B units immersed in the good solvent. The stars with $y > x$ exhibit considerably smaller sizes, although they are still slightly higher than those of $x = y$ stars with the same f.

The results for $\langle S^2 \rangle$ and Γ_2 contained in Table 1 and those corresponding to the rest of the values of Φ_B have been included in fits versus N, to obtain numerical exponents and proportionality constants consistent with eqs 4a and 4b. These fits have been performed for the different architectures and solvent cases. For case a (good solvent), the results for exponent ν, $\nu \cong 0.58-0.6$, are always close to the theoretical value. Only the case $x = 6$, $y = 6$ shows a slightly smaller value, $\nu \cong 0.57$, when $\Phi_B \cong 0.5$, due to the higher finite size effects present in stars with many arms of similar lengths. The proportionality constants in eqs 3a and 3b decrease for higher f, as an obvious effect of the topology on the chain size and vary with Φ_B, as is illustrated in Figure 1 for $A_S(f, x, \Phi_B)$. Because all interactions are equivalent in case a, different values of x and Φ_B correspond to homopolymer star chains with two types of arms simply differentiated by respective lengths. The curves exhibit a minimum at $\Phi_B = 0.5$ for the stars with $x = y$ (same number of A and B arms), which behave as homopolymer stars of f units. It also shows maxima at $\Phi_B = 0$ and 1, where the molecules are in this case totally equivalent to homopolymer stars of $x = y = f/2$ arms (the other $f/2$ arms are of infinitesimally short relative lengths). The minimum becomes smoothed or even tends to disappear for stars with $x \neq y$, because the two limits for $\Phi_B = 0$ and 1 also correspond to homopolymer stars, but now with different numbers of arms x and y, and therefore, the main feature of the variation with Φ_B is now the net increase or decrease between these two limits.

For the case b (common Θ solvent), the results for ν are close to the theoretical value $\nu = 0.5$ for ideal chains (which is also the theoretical result expected when only heterointeractions are present[4]), being slightly smaller for the $x = y = 6$ star. The values of the proportionality constant are ca. 25−30% higher than those of case a, but they follow similar patterns in their variation with Φ_B (the decrease of the size due to the lack of excluded volume effects is manifested through the decrease of exponent ν, not through the values of these constants). Case c shows more differences in the variation of ν and the proportionality constant with Φ_B. Thus, $\Phi_B = 0$ corresponds now to a star of x arms in a Θ solvent (ideal

Table 1. Simulation Data for the Sizes and Second Virial Coefficients at the Particular Composition Value $\Phi_B = 0.5$ for Different Miktoarms Architectures and Solvent Cases

		solvent case							solvent case					
		good (*a*)		common θ (*b*)		selective (*c*)			good (*a*)		common θ (*b*)		selective (*c*)	
type	*N*	$\langle S^2 \rangle$	Γ_2	$\langle S^2 \rangle$	Γ_2	$\langle S^2 \rangle$	Γ_2	*N*	$\langle S^2 \rangle$	Γ_2	$\langle S^2 \rangle$	Γ_2	$\langle S^2 \rangle$	Γ_2
AB	81			16.69(4)	308(1)	20.81(6)	536(1)	181	65.55(8)	3121(3)	37.30(8)	1042(5)		
	85	26.58(4)	832(1)	17.46(4)	330.8(7)			201					58.0(3)	2461(6)
	91	28.84(4)	937.0(9)	18.75(5)	367.8(4)	23.9(1)	648(3)	211					61.3(1)	2690(10)
	109	35.77(8)	1285.2(8)					217	81.3(1)	4294(5)			62.8(2)	2796(11)
	121	40.43(6)	1541(2)	24.93(7)	567(2)	32.72(6)	1048(4)	241	92.0(3)	5145(10)	49.9(1)	1616(2)		
	141			29.18(5)	717.1(4)			289	113.7(3)	7075(16)				
	145	50.3(1)	2118(4)					325	130.7(2)	8671(9)				
	151			31.09(8)	796(3)	41.91(9)	1525.2(9)	337	137.1(2)	9233(11)				
	161			33.15(5)	872.5(3)	45.0(2)	1704(7)							
A2B	73	18.06(2)	605.9(3)					141			24.28(6)	712(2)		
	81			13.96(4)	305.96(8)	18.00(9)	520(2)	145	40.70(8)	2010(2)				
	85	21.68(3)	793(1)					161			27.62(5)	875(2)	48.5(3)	2178(2)
	109	29.05(7)	1217.8(6)					201					50.6(2)	2404(11)
	121	32.82(4)	1463(1)	20.79(6)	569(2)	28.52(5)	1028(3)	289	92.01(3)	6707(7)				
A2B2	73	13.85(3)	560.6(9)					141			19.18(2)	705.6(6)		
	81			11.04(2)	302.9(3)	13.29(4)	492(1)	145	30.94(9)	1849(3)				
	85	16.51(2)	729.4(7)					161			21.80(8)	862(1)	28.36(9)	1558(5)
	109	22.0(1)	1123(1)					201					36.37(5)	2268(9)
	121	25.03(3)	1349(3)	16.50(5)	559(1)	20.82(9)	970.7(3)	217	49.90(7)	3742(7)				
A3B	61	13.16(4)	420.7(3)	9.50(3)	193.0(3)	12.04(5)	314(1)	121	29.49(9)	1387(2)	18.81(4)	547(1)	26.3(1)	993(8)
	73	16.24(7)	575(1)					145	36.65(5)	1895(2)				
	85	19.52(4)	750.4(8)					151			23.63(8)	762.8(3)	33.8(2)	1436(4)
	91			14.26(4)	353.8(8)	19.26(8)	619.6(3)	211					50.4(3)	2541(8)
	109	26.17(8)	1157(2)					217	58.9(1)	3844(7)				
AB3	61					10.52(5)	303.5(8)	151					27.8(1)	1368(3)
	91					15.93(2)	583.2(4)	211					39.3(1)	2379(3)
	121					21.8(1)	941(2)							
A4B	65			9.57(2)	204.2(3)			121	27.79(7)	1323(3)	17.81(5)	524(1)		
	73	15.33(7)	549(2)					145	34.4(1)	1806(2)				
	81			12.05(3)	286.2(4)			161			23.6(1)	806(2)		
A3B3	61			6.25(1)	180.6(6)			121	17.95(3)	1150(2)	12.21(1)	511(1)	15.09(3)	852(3)
	73	10.04(2)	481.9(6)					145	22.20(3)	1578(2)				
	85	11.95(2)	627(1)					151			15.15(3)	713(2)	19.33(4)	1239(1)
	91			9.24(2)	331.8(6)	11.10(3)	532.3(7)	181						
	97							217					28.74(4)	2267.8(9)
	109	15.91(3)	961(2)											
A4B2	65			7.24(2)	200.4(8)			145	24.5(1)	1622(3)				
	73	11.04(2)	495.5(4)					161			17.70(6)	791(2)	24.3(1)	1451.5(1)
	81			9.00(2)	279.5(8)	11.24(4)	461(1)	201					31.2(1)	2105(6)
	121	19.78(6)	1181(4)	13.31(4)	513.2(8)	17.65(5)	902(2)							
A2B4	81					10.14(4)	429(2)	161					21.09(9)	1345(5)
	121					15.55(7)	827(2)	201					26.9(1)	1934(5)
A6B6	73	5.88(1)	336.6(3)					181	16.05(3)	1561(4)	10.32(2)	682(6)		
	85			5.066(5)	225.5(3)			241	22.32(5)	2564.3(8)	13.62(2)	1040(9)		
	97	8.02(2)	542.6(5)					301	29.00(6)	3798(4)				
	121	10.22(2)	784.3(9)	7.06(1)	378(2)									

behavior), whereas $\Phi_B = 1$ describes a star of *y* arms in a good solvent. Consequently, ν varies for values close to $\nu = 0.5$ for $\Phi_B = 0$ to values close to $\nu = 0.59$ for $\Phi_B = 1$. Some results for this exponent obtained from simulation data for the star sizes are shown in Figure 2. The variation is not uniform, and we have found that for $\Phi_B = 0.5$ most values of ν are closer to the $\nu = 0.59$ limit than to $\nu = 0.50$, with this change being less drastic for stars with $y > x$, where the B arms are short for this compositional fraction and they cannot contribute as much to the global size. It can be expected that the $\nu \cong 0.59$ value should be reached for any chain containing homointeractions, and therefore, all of the numerical differences with respect to this limit reflect finite size effects for the given star architecture that will eventually vanish for higher (much higher in some cases) values of *N*. Therefore, the present simulation data corresponding to $\Phi_B < 0.5$ for selective solvents are clearly affected by these effects. The proportionality constants shows a decrease from the Θ solvent values for $\Phi_B = 0$ to the good solvent values for $\Phi_B = 1$ (which are about 25% smaller as described above in our comparison of cases *a* and *b*). The minima of the variation of the constants with Φ_B are smoothed or totally suppressed due to this net decrease.

In addition, the simulation results have allowed us-to-obtain ratios g_S, g_A, and parameter Ψ^* for the different values of *N*, star architectures, and solvent cases. These quantities show a weak variation with *N* for each given star architecture and solvent case, and they can actually be extrapolated to their long-chain limit. In fact, the results corresponding to relatively high values of *N* ($N \geq 100$) show an overlap of their numerical uncertainties. Therefore, we have estimated the long-chain limits as arithmetic means over these overlapping values. We recognize that some slight system-

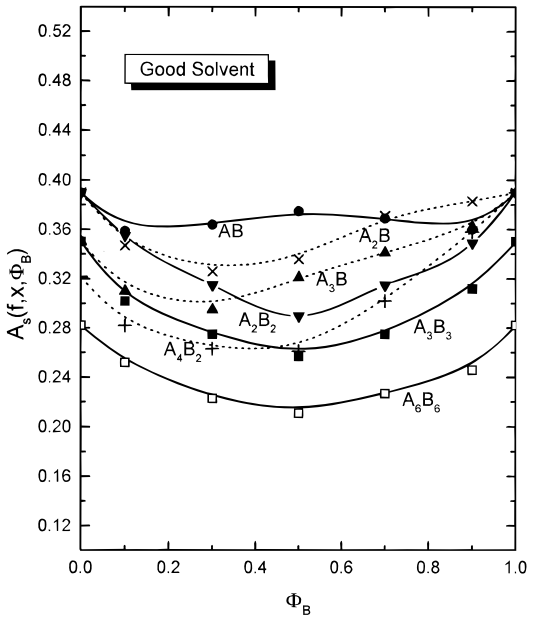

Figure 1. $A_S(f, x, \Phi_B)$ vs Ψ^* vs Φ_B for miktoarms of different architectures immersed in a good solvent (case a): ●, AB (linear diblock); ×, A_2B; ▲, A_3B; ▼, A_2B_2; ■, A_3B_3; +, A_4B_2; and □, A_6B_6. Solid and dash lines are guides for the eye.

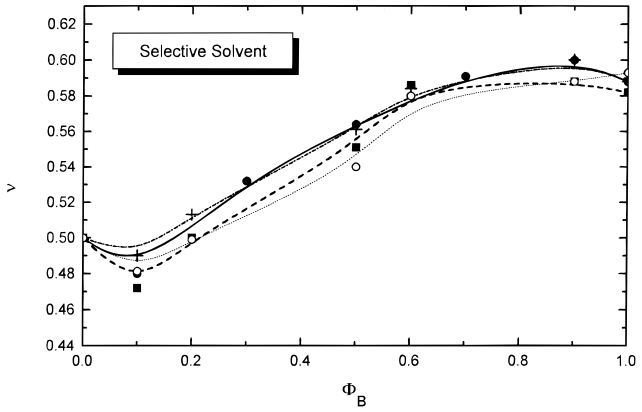

Figure 2. ν (obtained from the size simulation data) vs Φ_B for miktoarms of different architectures immersed in a selective solvent (case c): ●, AB (linear diblock); ○, A_2B_4; ■, A_3B_3; and +, A_4B_2. Different lines are guides for the eye.

atic variation with N can be neglected though this procedure in some particular cases, but due to the great diversity of architectures and cases explored here, we have decided to maintain this general criterion, in the confidence that the final extrapolations are obtained with sufficient accuracy (less than 3% error) for the purposes of the present work.

The long-chain values for ratio g_S versus the compositional fraction Φ_B in case a (good solvent) are shown in Figure 3. According to arguments based on the renormalization group theory[6,8] and according to previous simulation data,[15,18] the value of ratio g_S for a uniform homopolymer star in a good solvent should be very close to that obtained for an ideal chain in the absence of interactions, which, for uniform stars, is given as

$$g_S(\text{ideal}) = (3f - 2)/f^2 \qquad (6)$$

This point has also been satisfactorily verified with the present simulation data for the particular values of Φ_B

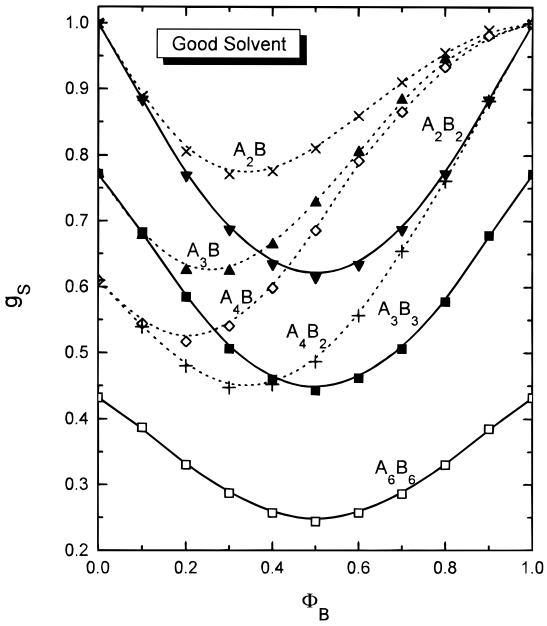

Figure 3. g_S vs Φ_B for miktoarms of different architectures immersed in a good solvent (case a): ×, A_2B; ▲, A_3B; ▼, A_2B_2; ■, A_3B_3; +, A_4B_2; ◇, A_4B; and □, A_6B_6. Solid and dash lines are guides for the eye.

that actually correspond to uniform stars. Then, the curves for molecules with the same total number of arms, f, but different values of x and y, show minima with a given common depth, which is also the value found in the uniform "homopolymer" limits A_f or B_f of curves for stars with total number of arms greater than this particular f. The minimum is placed at $\Phi_B = 0.5$ for $x = y$, whereas for $x \neq y$, it is placed at the value of Φ_B that also correspond to a uniform star. In these cases, the curves have a smoother aspect due to the smaller difference between the minimum and the ratio value in the limit $\Phi_B = 0$ or 1 that is closer to that minimum. These features are again simply explained by the reduction of size for homologous star chains of higher number of arms.

Parameter Ψ^*, shown in Figure 4, shows the opposite trend, because it is size-independent and only reflects the effect of the density of intermolecular interactions on the second virial coefficients. It is clear that this density of interactions is higher for the stars with higher numbers of arms, and therefore, the variation of Ψ^* with the compositional fraction shows a maximum with fixed value for the intermediate cases of a uniform stars with $f = x + y$ arms. Two minima are placed at the limits $\Phi_B = 0$ and 1 corresponding to uniform stars of x or y arms. The maximum corresponds to $\Phi_B = 0.5$ if $x = y$ or a value closer to the highest limit $\Phi_B = 0$ or 1 for $x \neq y$. Each maximum also coincides with the homopolymer limits A_f or B_f in curves of miktoarms with numbers of arms greater than f. It should also be remarked that the good solvent data of Ψ^* for values of Φ_B that correspond to uniform stars can be compared directly with existing experimental data[8] and with simulation data obtained with other theoretical models[9,10] and have been analyzed in detail in previous work.[11]

Figure 5a shows the simulation results for ratio g_A. The curves corresponding to g_S and g_A have similar qualitative aspects. According to eqs 2, 3a, and 3b

$$g_\Psi \equiv (\Psi^*)_{\text{mikto}}/(\Psi^*)_{\text{diblock}} = g_A/(g_S)^{3/2} \qquad (7)$$

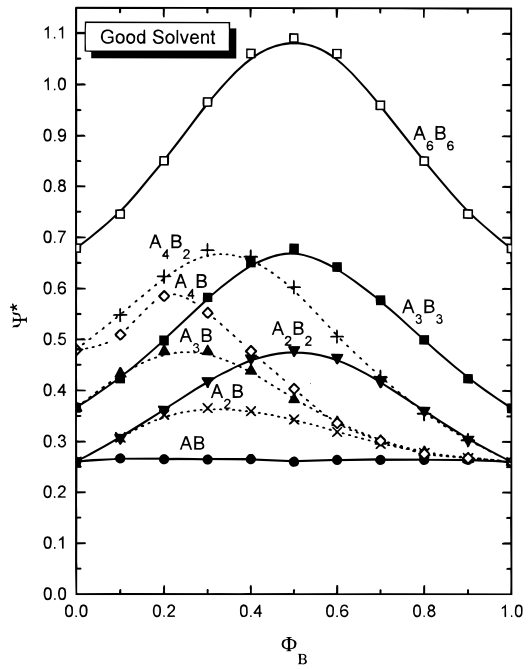

Figure 4. Ψ* vs Φ_B for miktoarms of different architectures immersed in a good solvent (case a): ●, AB (linear diblock); ×, A_2B; ▲, A_3B; ▼, A_2B_2; ■, A_3B_3; +, A_4B_2; ◇, A_4B; and □, A_6B_6. Solid and dash lines are guides for the eye.

and, because in the present case $(\Psi^*)_{\text{diblock}}$ is constant, the variation of g_S and Ψ* with Φ_B determine g_A. The variation of g_S is clearly predominant in the present case, and the curves show well-defined minima. The influence of g_Ψ is, nevertheless, manifested through the flatter variation of the g_A data with respect to the g_S curves. Consistently with the g_S and g_Ψ curves, g_A also shows a common (minimum) value for the different uniform stars with the same total number of arms but different x and y, and this value also is found in the corresponding homopolymer limits A_f or B_f of other miktoarms with more arms.

Figure 6 contains numerical values for ratio g_S but now corresponding to a common Θ solvent (case b). The aspect of the curves is similar to case a. Therefore, we can again observe the presence of minima of the same depths for miktoarms of the same number of arms, but with different values of x and y, placed at the composition values for which the stars are uniform. However, the explanation of this feature is not so obvious as in case a, where all interactions were identical. This seems to show that the relative increase in the size due to the presence of heterointeractions is practically the same in any uniform miktoarm of a given number of arms with respect to the homologous diblock linear chain, and therefore, the minima in the variation of the ratios do not depend on Φ_B. Therefore, the heterointeractions, when added to a uniform star chain and to a homologous linear chain, give rise to relative expansion effects only depending on the total number of arms. This feature is underlined by observing the trends of the simulation curves toward the limits $\Phi_B = 0$ and 1. Instead of reproducing the results predicted by eq 6 for ideal homopolymers with only x or y arms, a smooth behavior is only consistent with slightly but noticeably higher limits values. These values also correspond precisely to the minima obtained with uniform stars with $f = x$ ($\Phi_B = 0$) or $f = y$ ($\Phi_B = 1$). Therefore, the apparent ratios g_S for $\Phi_B = 0$ or 1 in case b (included in Figure 6) can be

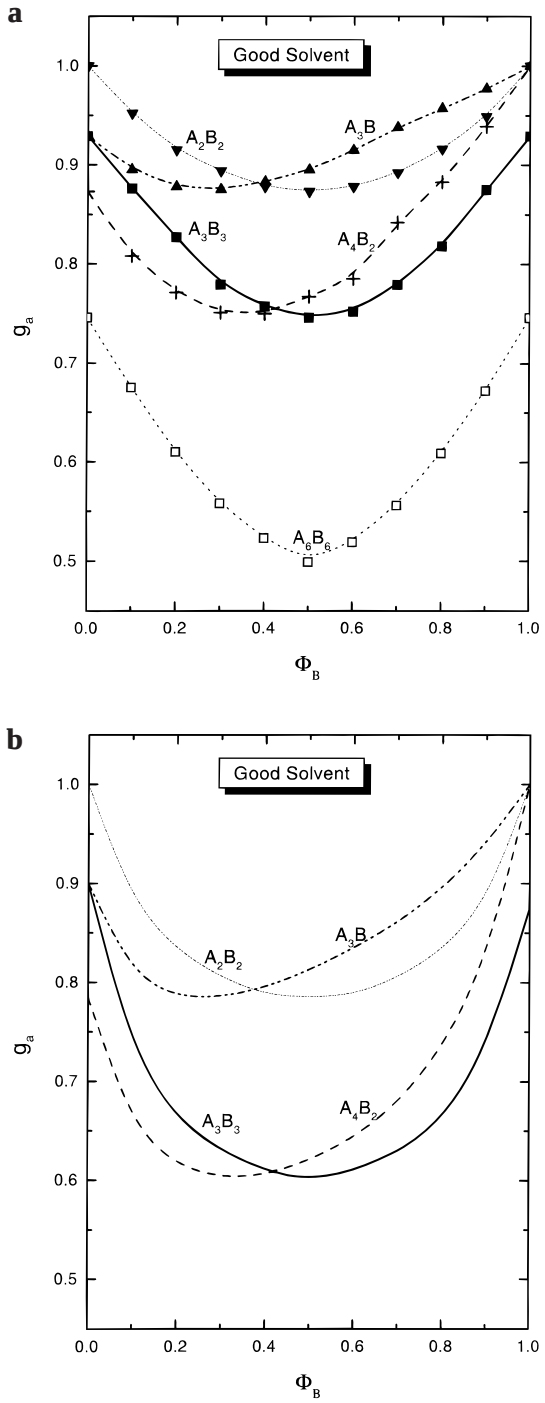

Figure 5. g_A vs Φ_B for miktoarms of different architectures immersed in a good solvent (case a). (a) Simulation values: ▲, A_3B; ▼, A_2B_2; ■, A_3B_3; (+): A_4B_2; and □, A_6B_6. Different lines are guides for the eye and also for comparison with theory. (b) Curves from a renormalization group theory[12] as indicated, with the same line codes as those in part a.

understood as describing the relative sizes of hypothetical uniform miktoarm and diblock chains where heterointeractions of a given type of arm (A or B) are still present, but their lengths are very short compared to those of the other type of arms. This ratio is similar to those obtained for the rest of uniform miktoarms in a common Θ solvent with the same number of arms f as x or y.

For any intermediate composition, the ratios g_S are also higher for case b than those for case a. The common Θ solvent case adds the heterointeractions to the ideal

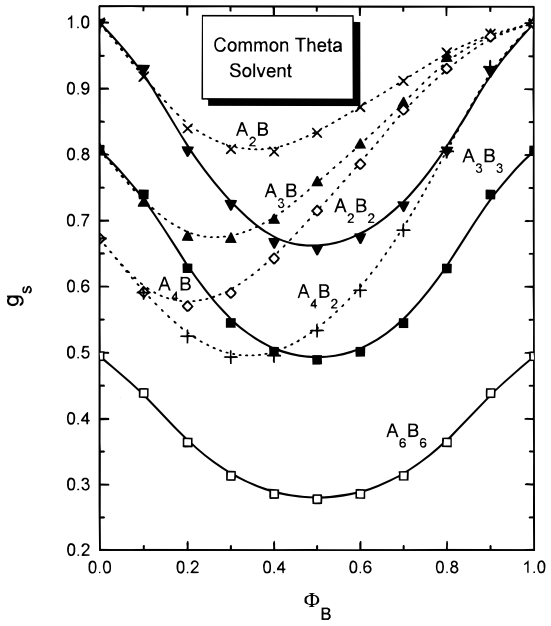

Figure 6. g_S vs Φ_B for miktoarms of different architectures immersed in a common Θ solvent (case b): ×, A_2B; ▲, A_3B; ▼, A_2B_2; ■, A_3B_3; +, A_4B_2; ◇, A_4B; and □, A_6B_6. Solid and dash lines are guides for the eye.

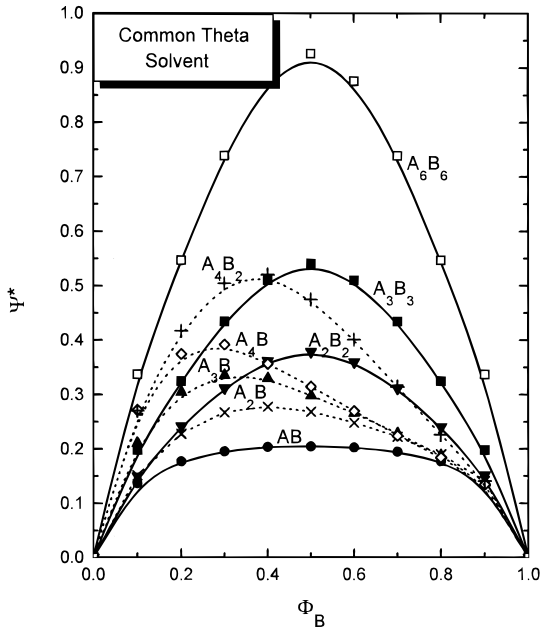

Figure 7. Ψ^* vs Φ_B for miktoarms of different architectures immersed in a common Θ solvent (case b): ●, AB (linear diblock); ×, A_2B; ▲, A_3B; ◇, A_4B; ▼, A_2B_2; ■, A_3B_3; +, A_4B_2; and □, A_6B_6. Solid and dash lines are guides for the eye.

chain. These heterointeractions tend to segregate the arms with different types of units, increasing the size of the arms. Because the ratios corresponding to stars with excluded volume between all units behave similarly to those of ideal chains, the increase of these ratios for case b, where only heterointeractions are present, can be conveniently explained. We should also mention that, as we have described in the Introduction, the present results have been obtained with a model for the Θ state that ignores core effects, as explained by the well-known scaling theory.[19] These effects may also give an important positive contribution to g_S.

The curves for parameter Ψ^* for case b are shown in Figure 7. They are considerably more abrupt than those in case a. The explanation of this feature is that, in the common Θ case, the apparent limits for $\Phi_B = 0$ and 1 seem to be close to $\Psi^* = 0$ (value included in Figure 7), despite the possible contributions from heterointeractions between very short arms of and very long arms of A or B types. Therefore, these apparent limits are considerably smaller than the finite value of Ψ^* for the same homopolymer stars in the good solvent case. Then, the change from $\Psi^* = 0$ to the maximum value for a common Θ solvent is always greater than the change in the good solvent case. Consequently, the change in g_Ψ is greater than that in case a for all of the miktoarm architectures. The values of the maxima for Ψ^* are, however, smaller, for case b than for case a, because the former case only include intermolecular heterointeractions. For the same reason, Ψ^* is smaller for case b over the whole range of values of Φ_B. The maxima again correspond to the values of Φ_B consistent with uniform miktoarms. It should be pointed out that differences between the maxima obtained in cases *a* and *b* are not very dramatic (about 20% for all of the architectures from the linear diblock copolymers up to the stars of 12 arms), which indicates the remarkable contribution of the heterointeractions in total intermolecular interactions and second virial coefficients of the uniform stars. It can also be observed that the values of Ψ^* for these uniform miktoarms are not only dependent on *f* but also depend on the particular values of *x* and *y*, being smaller when Φ_B is closer to 0 or 1 (which is consistent with the apparent $\Psi^* = 0$ limits for $\Phi_B =$ 0 or 1). This represents a difference with respect to the behavior of Ψ^* in case a and with respect to the ratio curves for g_S in the present case.

The simulation curves for ratio g_A (contained in Figure 8a) are remarkably flatter for the intermediate compositional fractions in case b than in case a. The elimination of interactions between units of the same type is surely the main cause of this behavior. From the numerical point of view, it can be argued that the stronger changes of Ψ^* and g_Ψ with the compositional fraction in case b balance more effectively the influence of factor $(g_S)^{3/2}$ in eq 7 (Ψ^* is practically constant for the linear diblock in the range $\Phi_B = 0.2-0.8$ in both cases a and b). Therefore, the g_A curves adopt a flat aspect. The limits of g_A for $\Phi_B = 0$ and 1 cannot be directly computed. Figure 8 contains rough estimations of these quantities from eq 7, and determining g_Ψ from the apparent slopes shown by the curves at $\Phi_B = 0$ in Figure 7,

$$g_\Psi(\Phi_B = 0, 1) = (d\Psi^*/d\Phi_B)_{mikto}/(d\Psi^*/d\Phi_B)_{diblock} \quad (8)$$

Actually, all our evaluations of this apparent limits for the common solvent case with *f* not greater than 6 give rough estimations of the limits around $g_A \cong 1$. For all of the intermediate compositional fractions, higher values of g_A are obtained for case b than for case a (similar to the g_S curves). The absence of interactions different from the heterointeractions in the case b for a common Θ solvent explains that the different architectures give second virial coefficients closer to the linear chains with the same Φ_B than in case a, where intermolecular interactions of all of the different types have to be considered. From the numerical point of view, both g_S and g_Ψ are higher for case b, and therefore, eq 7 determines that g_A should be also higher.

Figures 9, 10, and 11a show the simulation values of g_S, Ψ^*, and g_A for miktoarms in a selective solvent (case

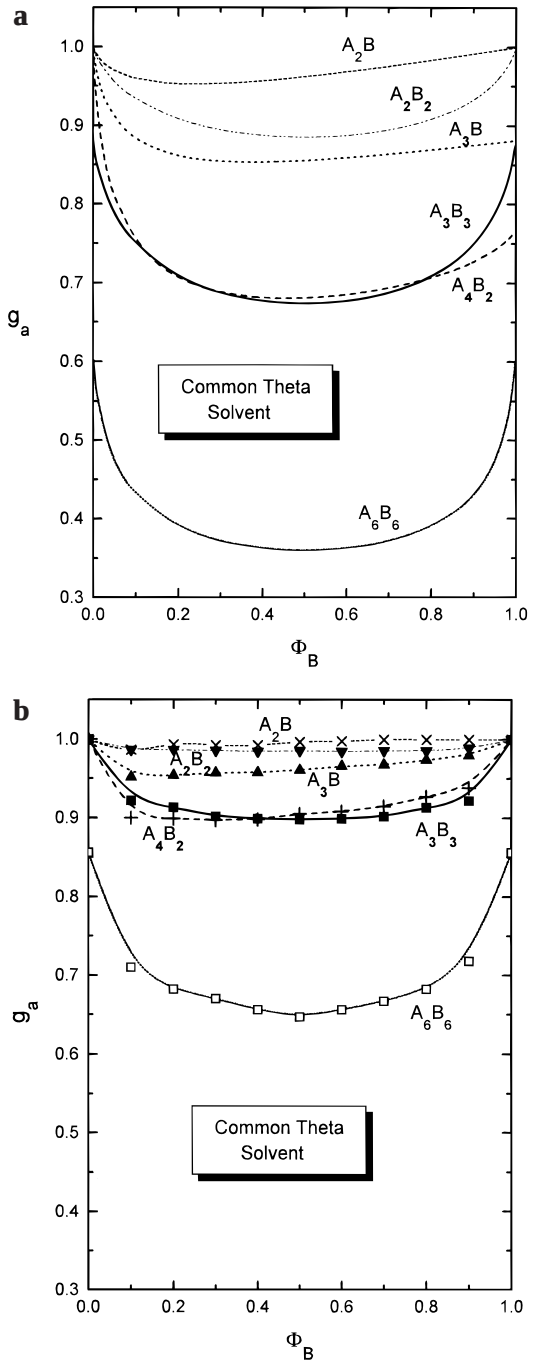

Figure 8. g_A vs Φ_B for miktoarms of different architectures immersed in a common Θ solvent (case b). (a) Simulation values: ×, A_2B; ▲, A_3B; ◇, A_4B; ▼, A_2B_2; ■, A_3B_3; +, A_4B_2; and □, A_6B_6. Different lines are guides for the eye and for comparison with theory. (b) Curves from a renormalization group theory[12] (see text) as indicated, with the same line codes as in part a.

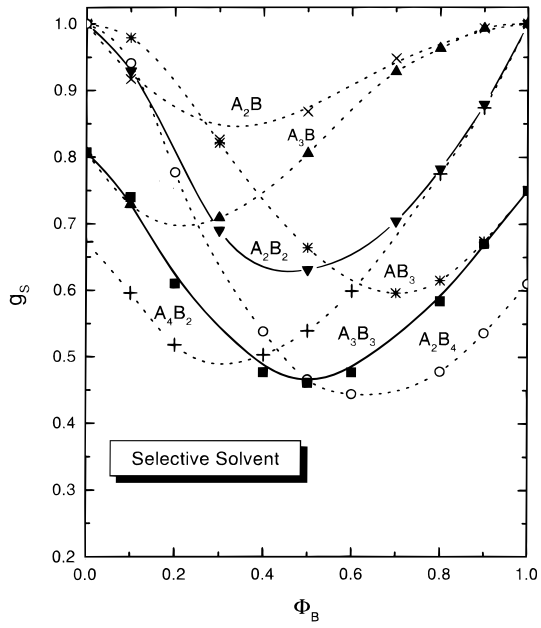

Figure 9. g_S vs Φ_B for miktoarms of different architectures immersed in a selective solvent (case c): *, AB_3; ×, A_2B; ▲, A_3B; ▼, A_2B_2; ■, A_3B_3; +, A_4B_2; and ○, A_2B_4. Solid and dash lines are guides for the eye.

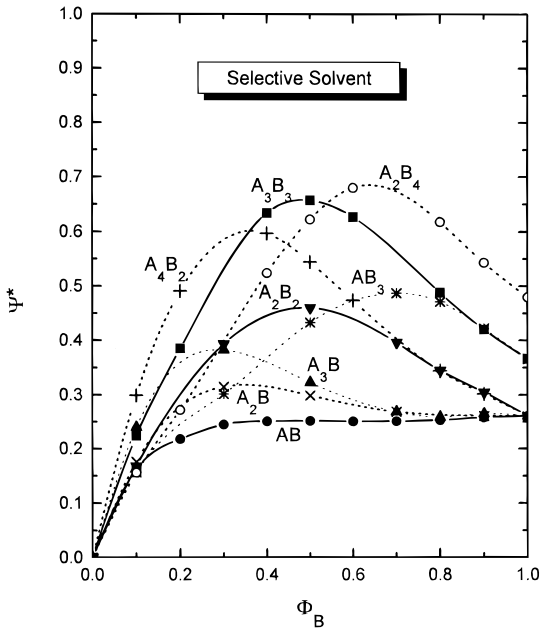

Figure 10. Ψ^* vs Φ_B for miktoarms of different architectures immersed in a selective solvent (case c): ●, AB (linear diblock); *, AB_3; ×, A_2B; ▲, A_3B; ▼, A_2B_2; ■, A_3B_3; +, A_4B_2; and ○, A_2B_4. Solid and dash lines are guides for the eye.

c). As we stated above, these values may show important finite size effects for $\Phi_B < 0.5$. The values of g_S and Ψ^* for the limit $\Phi_B = 0$ are plotted assuming that they should agree with the corresponding apparent limits for case b. The limit $\Phi_B = 1$ corresponds to the case of a homopolymer star of y arms in good solvent, and the results in this limit should be the same as those obtained for case a. The values of Ψ^* and ratio g_A for case c are always intermediate between these two cases with respect to both the aspect of the curves and the quantitative data for a given Φ_B. It should be considered that these quantities are directly related with the second virial coefficient and are mainly determined by the number of interactions. However, the behavior of g_S is more subtle, and it is observed in most cases that the values of g_S for selective solvents are similar or even higher than those of the same miktoarm star in a common Θ solvent (and therefore clearly higher than those for the same star in a good solvent for all the architectures). In case a, interactions between all units are considered, but as we explained before, these interactions seem to cancel for star and linear chains in ratio g_S so that this ratio is smaller than that for case b. Apparently, the presence of heterointeractions together with homointeractions only for a type of units sometimes give a positive contribution for g_S, with

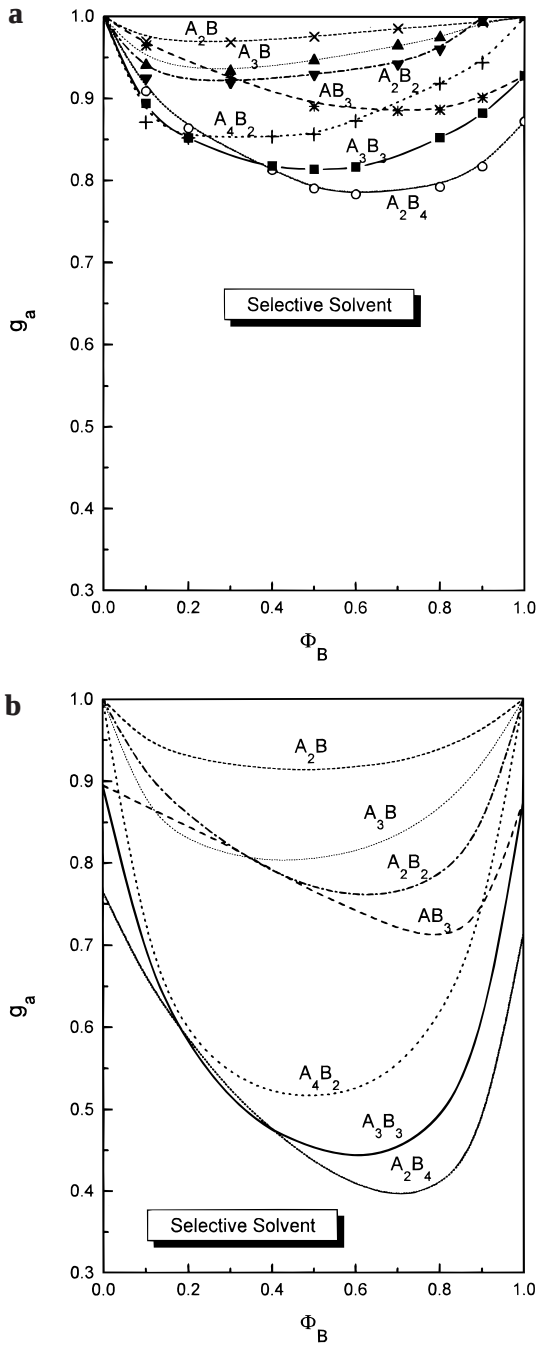

Figure 11. g_A vs Φ_B for miktoarms of different architectures immersed in a selective solvent (case c): (a) Simulation values: ×, A_2B; ▲, A_3B; ▼, A_2B_2; ■, A_3B_3; *, AB_3; +, A_4B_2; and ○, A_2B_4. Different lines are guides for the eye and for comparison with theory. (b) Curves from a renormalization group theory[12] as indicated, with the same line codes as in part a.

respect to case b, where only the heterointeractions are present.

Figures 5b, 8b, and 11b contain theoretical curves for the variation of the ratio g_A with the compositional fraction that allow for a direct comparison with the present Monte Carlo results. These theoretical values have been obtained[12] by using a simple perturbation scheme up to the second order in the perturbation parameters. General analytical expressions are obtained for A_2 for miktoarm and diblock copolymers in terms of these parameters. Taking into account the fixed-point values of the interaction parameters for the different solvent cases, first-order expressions in the dimensional parameter ϵ are derived for the ratio g_A. To avoid unphysically negative values of g_A for high values of the total number of arms, these first-order expansions have been exponentiated. In the cases where the star architectures correspond to uniform homopolymer stars, e.g., $x = y$ with $\Phi_B = 0.5$, in a good solvent, the theoretical results for g_A are much smaller than existing experimental data[8] and some previous Monte Carlo values.[9,10] An improvement is introduced[12] by rewriting the analytical results for A_2 in a closed form, determined from the first two terms of the perturbation expansion, according to a method previously followed by Kosmas and Kosmas.[13] For the simpler case of a single interaction parameter u, they obtained $A_2 = uN_{AV}\{1 + 8u[\ln M + F(f)]\}^{-1/2}$, where $F(f)$ is a function depending on the star architecture. The parameters 8 and $-1/2$ were determined from the first two terms of the series expansion, and their values are consistent with the third-order terms. The theoretical curves contained in Figure 5b actually correspond to this improved version of the procedure. It is shown, however, that the present Monte Carlo results contained in Figure 5a are always higher than those of the theory predictions, although the qualitative trends followed by the Monte Carlo data and the theoretical curves are remarkably similar for each type of miktoarm architecture.

In the simpler cases where the miktoarms are reduced to uniform homopolymer stars in a good solvent, the performance of these theoretical calculations for good solvents can be compared with the results obtained by Douglas and Freed.[6] These authors used also an exponentiation method. Their calculations agree better with experimental results and Monte Carlo data for small number of arms (although they also show some differences with respect to these values), but they become unphysically negative for $f \geq 18$.

Figure 8 allows for a similar comparison of the theoretical curves with our Monte Carlo data for the case of the common Θ solvent case. We have verified that the theoretical curves reported previously[12] for this case using the exponentation procedure are always much smaller than the Monte Carlo data. For this reason, we have rewritten the analytical expressions for A_2 in terms of a closed expression similar to that accomplished previously in the good solvent case, following the Kosmas procedure. The theoretical curves in Figure 8b actually correspond to the improved expression, which, again, yields an adequate reproduction of the qualitative shape of the curves, but it predicts quantitative results still considerably smaller than the Monte Carlo data. The theory predicts that the limits $\Phi_B = 0$ and 1 for g_A are actually governed by the number of arms of the shorter chains. The rather flat aspect of the present simulation curves at intermediate values of Φ_B (also shown by the theoretical curves except when they are very close to the limits) cannot permit a verification of this point. According to the analysis described above, the limits of our simulation curves for g_S are apparently governed by the number of arms of the longer chains. However, the higher slopes shown by the Ψ^* versus Φ_B curves with $x > y$ in the $\Phi_B = 0$ limit (and the corresponding opposite case) give higher values of g_Ψ through eq 8 for these molecules. According to eq 7, these g_Ψ can possibly overcome the effect of the smaller g_S values in the limits of the g_A curves.

Figure 11b contains the theoretical curves corresponding to selective solvents. These results have been directly obtained from the exponentiated expression (an improved expression is not available), and consequently, they show an even larger quantitative difference with respect with the higher Monte Carlo data. However, because of the variety of different architectures for this particular solvent case and the asymmetry exhibited by many of the curves, the qualitative similarity between theoretical and Monte Carlo variations with Φ_B is particularly underlined (for instance, one can observe how curves for different star cases cross each other at values of Φ_B that are remarkably similar for the theory and Monte Carlo data). Our general conclusion for the three solvent cases is that, given the qualitative description of the data features by the theoretical method, a further improvement in theory can probably be performed by taking the present Monte Carlo data as a guiding reference. Douglas and Freed[20] have performed a renormalization group theory analysis of diblock copolymers. They considered limit values where exact results are known, using this nonperturbative information to guide the resummation whenever possible. We hope that a similar approach can be applicable to the miktoarm star properties.

Acknowledgment. This work has been partially supported by the Spanish−Greek scientific cooperation program, Action VI, and also by Grant PB98-0791 of the DGESIT (Ministerio de Educación y Cultura), Spain.

References and Notes

(1) Grest, G. S.; Fetters, L. J.; Huang, J. S.; Richter, D. *Adv. Chem. Phys.* **1996**, *94*, 67.
(2) Freire, J. J. *Adv. Polym. Sci.* **1999**, *143*, 35.
(3) Hadjichristidis, N.; Pispas, S.; Pitsikalis, M.; Iatrou, H.; Vlahos, C. *Adv. Polym. Sci.* **1999**, *142*, 71.
(4) Vlahos, C.; Horta, A.; Freire, J. J. *Macromolecules* **1992**, *25*, 5974.
(5) Vlahos, C.; Horta, A.; Hadjichristidis, N.; Freire, J. J. *Macromolecules* **1995**, *28*, 1500.
(6) Douglas, J.; Freed, K. *Macromolecules* **1984**, *17*, 2344.
(7) Gray, C. G.; Gubbins, K. E. *Theory of Molecular Liquids*; Clarendon Press: Oxford, 1984; Vol. 1.
(8) Douglas, J.; Roovers, J.; Freed, K. *Macromolecules* **1990**, *23*, 4168.
(9) Ohno, K.; Shida, K.; Kimura, M.; Kawazoe, Y. *Macromolecules* **1996**, *29*, 2269.
(10) Rubio, A.; Freire, J. J. *Macromolecules* **1996**, *29*, 6946.
(11) Rubio, A.; Freire, J. J. *Comput. Theor. Polym. Sci.*, in press.
(12) Vlahos, C.; Hadjichristidis, N. *Macromolecules* **1998**, *31*, 6691.
(13) Kosmas, M. K.; Kosmas, A. *Polymer* **1986**, *27*, 1359.
(14) Baumgärtner, A. *J. Chem. Phys.* **1982**, *76*, 4275.
(15) Freire, J. J.; Rey, A.; Bihop, M.; Clarke, J. H. R. *Macromolecules* **1991**, *24*, 6494.
(16) Li, B.; Madras, N.; Sokal, A. *J. Stat. Phys.* **1995**, *80*, 661.
(17) López Rodriguez, A.; Freire, J. J. *Mol. Phys.* **1988**, *63*, 591.
(18) Rey A.; Freire, J.; García de la Torre, J. *Macromolecules* **1987**, *20*, 342.
(19) Daoud, M.; Cotton, J. P. *J. Phys. (Paris)* **1982**, *43*, 531.
(20) Douglas, J.; Freed, K. *J. Chem. Phys.* **1987**, *86*, 4280.

MA9913156